Carbon 95 (2015) 659–663

Contents lists available at ScienceDirect

Carbon

journal homepage: www.elsevier.com/locate/carbon

Electron–hole recombination dynamics in carbon nanodots

Vanthan Nguyen [a, b], Jinhai Si [a, *], Lihe Yan [a], Xun Hou [a]

[a] Key Laboratory for Physical Electronics and Devices of the Ministry of Education and Shaanxi Key Lab of Information Photonic Technique, School of Electronics and Information Engineering, Xi'an Jiaotong University, Xi'an 710049, China
[b] Le Quy Don Technical University, Hanoi 7EN-248, Viet Nam

ARTICLE INFO

Article history:
Received 3 April 2015
Received in revised form
12 August 2015
Accepted 21 August 2015
Available online 25 August 2015

ABSTRACT

Since their discovery, carbon nanodots (C-dots) have attracted great interest due to their strong photoluminescence (PL). Yet a full understanding of the mechanisms for PL from C-dots is still under debate. In this work, we analyzed the evolution of the time-resolved PL spectra of C-dots using picosecond time-resolved spectroscopy to explore the carrier dynamics in C-dots. Our results suggest two different pathways of electron–hole radiative recombination, each with distinct relaxation time scales: a relaxation of carriers from carbogenic core onto the surface states with a slow decay (>14 ns) and direct radiative recombination of carriers on the surface states with a fast decay (~1.3 ns). The slow decay at short-wavelength emissions is dominant due to the effective relaxation from the carbogenic core onto the surface states, while the fast decay is dominant at long-wavelength emissions. An explanation for the excitation-dependent and independent PL properties of C-dots is also presented here using this carrier dynamic model.

1. Introduction

Carbon nanodots (C-dots) are a novel carbon-based nanomaterial with sizes below 10 nm and have attracted considerable attention because of their unique combination of intense photoluminescence (PL), high water solubility, low toxicity, and excellent biocompatibility [1,2]. The first C-dots were discovered in 2004 by purifying single-walled carbon nanotubes through preparative electrophoresis [3]. Since their initial discovery, there has been significant progress in understanding the synthesis, properties, and applications of C-dots. Currently, C-dots are readily produced on large scales by several tunable methods [4–7]. Therefore, C-dots offer great potential for a broad range of applications, including biological imaging [8,9], drug delivery [10], sensors [8], photovoltaics [11], light-emitting diodes [12–14], and lasers [15].

Although great efforts have been made to investigate the fluorescence mechanisms of C-dots, the origin of their fluorescence remains to be a contentious topic. Several previous studies demonstrated the fluorescence of C-dots consists of two components. One originates from their intrinsic carbogenic core and the other stems from the presence of surface functional groups (i.e. surface states) [16–20]. Due to the relaxation of photogenerated carriers from the carbogenic core onto the surface states, the recombination lifetime progressively lengthens with increasing emission wavelength [18,21,22]. However, the fluorescence of C-dots is more complex than this simplified mechanism and it cannot explain several spectroscopic properties of C-dots, e.g. the recombination lifetime decreases at long-wavelength emissions [20–22]. Additionally, some C-dots are excitation-independent at short wavelengths but excitation-dependent at long wavelengths and the emission red shifts [16,17,22].

In this paper, we report on both the picosecond time-resolved fluorescence and the carrier dynamics of typical C-dots, allowing us to analyze the evolution of the time-resolved PL spectra. We propose a two-pathway model of the electron–hole radiative recombination in C-dots, each with a distinct relaxation time scales. There is a slow decay for the relaxation of carriers from carbogenic core onto the surface states, and a fast decay for the direct radiative recombination of carriers on the surface states. The relaxation from the carbogenic core onto the surface states is dominant at short-wavelength emissions, while the direct radiative recombination of carriers on the surface states is dominant at long-wavelength emissions. This result provides new fundamental insights into the PL mechanism of C-dots and helps explain their debated spectroscopy properties.

* Corresponding author.
E-mail address: jinhaisi@mail.xjtu.edu.cn (J. Si).

http://dx.doi.org/10.1016/j.carbon.2015.08.066
0008-6223/

2. Experimental

C-dots were synthesized via femtosecond laser ablation of graphite powder in a polyethylene glycol (PEG_{200N}) solution [23]. This method is chemically "clean" with essentially no contaminants and reduced byproduct formation, giving it a significant advantage over other techniques [24,25]. Furthermore, to simplify physical process and focus solely on the PL mechanism, C-dots were formulated with uniquely steady-state PL properties by minimalizing the surface functional groups. Typically, 20 mg of carbon powder, with a mean size of 400 nm, was dispersed into 50 ml of PEG_{200N} via ultrasonication. Next, ~10 ml of the suspension was put into a glass beaker (outside diameter × height: 25 mm × 35 mm) for laser irradiation. The laser beam (Ti:sapphire femtosecond laser system, central wavelength: 800 nm, pulse duration: 150 fs, and repetition rate: 1 kHz) was focused into suspension at a laser fluence of 500 J/cm^2 by 25 mm lens for about 3 h. During the laser irradiation, a magnetic stirrer was used to prevent gravitational settling of the suspended powders. After laser irradiation, the solution was centrifuged and the C-dots were obtained from the supernatant.

Transmission electron microscopy (TEM) and high resolution transmission electron microscopy (HRTEM) images of the C-dots were obtained via a high resolution transmission electron microscopy (model JEM-ARM200F). Through image analysis, the average diameter and size distribution was determined for ~1000 C-dots. A U-3010 spectrophotometer (Hitachi) was employed to measure the absorption spectra of the samples. The Fourier transform infrared spectroscopy (FTIR) was performed on a VERTEX 70 (Bruker) using KBr pellet method. A small droplet of supernatant containing as-prepared C-dots was deposited on KBr pellet and dried by placing the pellet in vacuum at 80 °C for 6 h. The emission and excitation spectra measurements were performed on a FLS920 spectrometer (Edinburgh) with the same bandwidth of 4 nm. The time-resolved PL spectra of C-dots were monitored with a 100 ps time resolution using a time-correlated single photon counting (TCSPC) system (FLS920 spectrometer) (excited by picosecond pulsed LEDs, pulse duration: <850 ps, repetition rate: 10 MHz).

3. Results and discussion

Using the aforementioned synthesis procedure, the C-dots in this study have a small size distribution, in the range of 1–2.5 nm, with mean size of 1.5 nm, as shown in Fig. 1a. The HRTEM image (Fig. 1b) indicates the C-dots contain a highly crystalline structure with lattice spacing of 0.21 nm. The spacing is very close to the (100) in-plane lattice spacing of graphite [26]. The UV–vis absorption spectrum of the as-prepared C-dots shows two different absorption peaks at 205 and 260 nm, which are attributed to the π–π^* transition of C=C double bond in the carbogenic core (Fig. 1c) [27,28]. The broad absorption ranging from 300 to 400 nm might be attributed to the surface functional groups on its surface. To ensure the purity of FTIR sample, a blank FTIR experiment of pure PEG_{200N} solution without C-dots following the same sample prepare procedure was conducted. The FTIR spectrum of the pure PEG_{200N} sample exhibits no absorption peak indicating that the solution is completely removed in the C-dots sample. Analysis of the FTIR spectrum of the C-dots shows that many surface functional groups are created on its surface (Fig. 1d). For example, there are stretching vibrations of the O–H bond at 3420 cm^{-1} [26], the C–H bond at 2920 cm^{-1} and 2855 cm^{-1} [29], the C=O double bond at 1630 cm^{-1} [26], and the C–O bond around 1000–1200 cm^{-1} [29]. To compare the difference between the FTIR spectra of C-dots and PEG_{200N}, FTIR spectrum of pure PEG_{200N} solution deposited on KBr pellet without drying was conducted. The FTIR spectrum of the C-dots shows new absorption peak of C=O double bond and a stronger absorption peak of C–O bond in comparison with that of PEG_{200N}, indicating that PEG_{200N} might be ionized or fragmented and further reaction with C-dots creating abundant surface functional groups.

The steady-state PL spectra of the as-prepared C-dots show two fluorescence peaks with coexistence of both excitation-independent and excitation-dependent properties (Fig. 2). The C-dots exhibit a strong peak at 405 nm with an excitation wavelength range between 280 and 380 nm, suggesting excitation independence. The fluorescence peak does not shift with increasing excitation wavelengths. However, when the excitation wavelength is further increased, $\lambda_{ex} \geq 400$ nm, the fluorescence peak shows clear evidence of a red shift and the intensity decreases sharply. The C-dots also have another apparent fluorescence peak at 325 nm, with an excitation range from 260 to 300 nm, indicating the existence of two dominant emission centers. This dual emission, centered at 325 and 405 nm, is present in the PL spectra when excited at 280 and 300 nm. The dual emission centers match very well with the two absorption bands in UV–vis absorption spectrum, in which the absorption band centered at 260 and 300–400 nm might be responsible for the emission centered at 325 and 405 nm, respectively. Increasing the excitation wavelength from 280 to 300 nm, the fluorescence peak intensity at 325 nm gradually decreases while the peak at 405 nm rapidly increases. This indicates that the emission centers are in turn excited and the dominant emission alternates when the excitation wavelength changes.

To explore the carrier dynamics in C-dots, the evolution of the picosecond time-resolved PL spectra of the as-prepared C-dots was monitored over a wavelength range of 325–465 nm at excitations of 273, 300, 343, and 369 nm. Each decay curve is fitted with a triple-exponential function; the best-fit parameters and average lifetimes are listed in Table 1. The fits of the fluorescence decays for the C-dots reach acceptable fit quality parameter ($\chi^2 < 1.15$) with randomly distributed around zero of residuals. The time-resolved PL spectra of the C-dots show different evolutions at short- and long-wavelength emissions. When excited by the 300 nm laser (Fig. 3a), PL dynamics detections at 325, 345, and 360 nm show slow decays (>14 ns). At longer emission wavelengths, i.e. 405, 435, and 465 nm, the PL dynamics are dominated by a faster decay (~1.3 ns). As shown in Table 1, the average lifetimes of the long-wavelength emissions are evidently shorter, 3.1–3.8 ns, when compared with those of the short-wavelength emissions, 14.2–17.4 ns. Similar PL dynamics, with two distinct relaxation time scales, are also observed at an excitation wavelength of 273 nm. The evolutions of the time-resolved PL indicate that two different pathways of electron–hole radiative recombination are responsible for the fast (long-wavelength emissions) and the slow (short-wavelength emissions) decays, respectively.

The dynamics of the PL emissions at 405, 435, and 465 nm, when exited by 343 nm laser, are shown in Fig. 3b. The percentage of the fast component (~1.3 ns) of the total fluorescence intensity is greater than 90%, and the average lifetime is evidently less than 2 ns. Comparing these results to the PL emissions when exited by the 300 nm laser, as shown in Fig. 3a, the fast decay of carrier recombination in the as-prepared C-dots becomes increasingly dominant with longer excitation wavelengths.

The PL dynamics detected at the fluorescence peak of 405 nm at different wavelength excitations are shown in Fig. 3c. The slow decays are gradually weakened by increasing excitation wavelength from 273 to 369 nm. As a result, the average lifetime decreases from 6.6 to 1.6 ns. It should be noted that the coexistence of both slow and fast decays is observed when the PL emissions are excited at 273 and 300 nm, while only fast decays exist in the decay curves at excitations of 343 and 369 nm. The percentage of the slow and fast decays changes with increasing excitation wavelength indicating

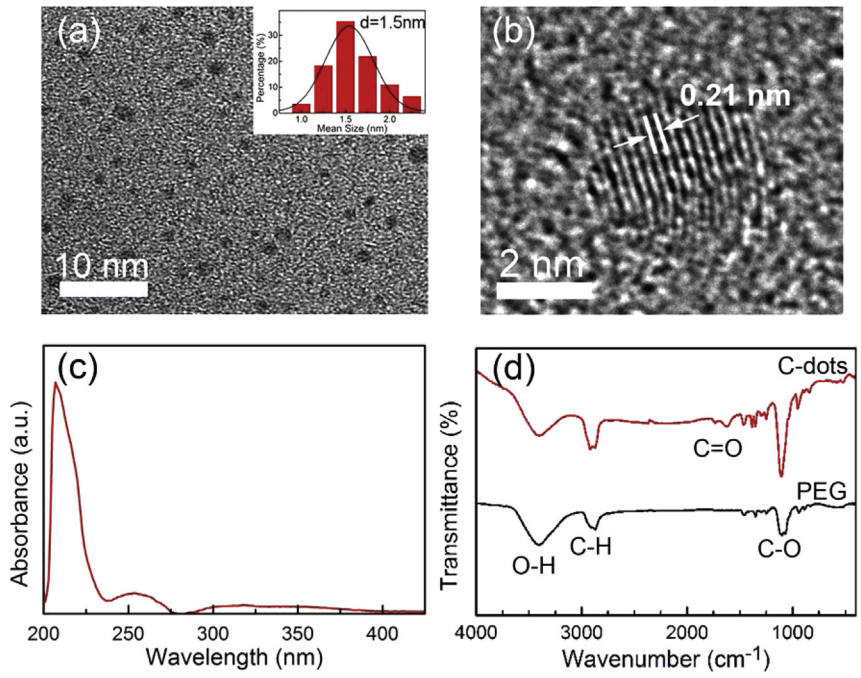

Fig. 1. (a) A TEM image of the as-prepared C-dots, the insert is the size distribution of the C-dots. (b) A typical HRTEM image of the C-dots. (c) The UV–vis absorption spectrum of the C-dots in solution. (d) The FTIR spectra of the C-dots and PEG_{200N}. (A color version of this figure can be viewed online.)

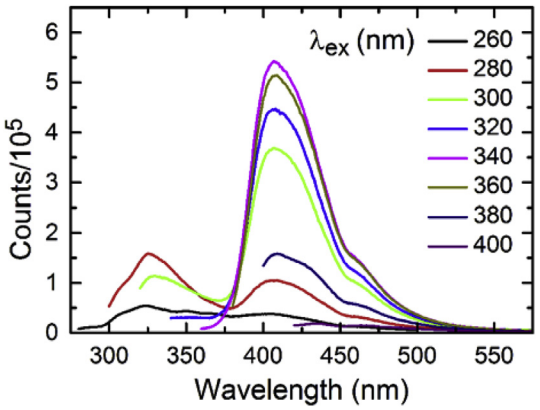

Fig. 2. The steady-state PL spectra of the as-prepared C-dots in solution. (A color version of this figure can be viewed online.)

Table 1
Triple-exponential fitting for time-resolved PL spectra of the C-dots at various detection wavelengths when excited at 273, 300, 343 and 369 nm.

λ_{ex}	λ_{em}	τ_1 (ns)	τ_2 (ns)	τ_3 (ns)	τ_{ave} (ns)
273 nm	325 nm	0.7 (3%)	4.9 (47%)	26.8 (50%)	15.7
	405 nm	1.1 (50%)	3.1 (15%)	15.9 (35%)	6.6
300 nm	325 nm	0.5 (6%)	4.6 (45%)	24.7 (49%)	14.2
	345 nm	0.7 (6%)	3.8 (30%)	25.4 (64%)	17.4
	360 nm	0.6 (8%)	3.4 (29%)	25.1 (63%)	16.8
	405 nm	1.3 (83%)	3.6 (4%)	14.6 (13%)	3.1
	435 nm	1.3 (82%)	6.0 (4%)	14.2 (14%)	3.3
	465 nm	1.3 (76%)	4.9 (6%)	13.9 (18%)	3.8
343 nm	405 nm	1.3 (96%)	8.5 (3%)	34.4 (1%)	1.8
	435 nm	1.3 (95%)	9.6 (4%)	36.5 (1%)	2.0
	465 nm	1.3 (91%)	4.4 (4%)	13.9 (5%)	2.1
369 nm	405 nm	1.3 (95%)	2.5 (3%)	16.3 (2%)	1.6

that both fast and slow decays occur in one C-dots and do not represent emission from separate groups of C-dots. The excitation spectrum of C-dots detected at 405 nm, shown in Fig. 3d, exhibit two excitation peaks around 300–320 and 330–360 nm. These results indicate that two distinct pathways of the electron–hole radiative recombination exist in the PL emission process of C-dots. The carrier recombination with slow and fast decays is dominant at short wavelength excitations and a fast decay is dominant at long wavelength excitations.

Contrary to previous studies [17,18], this work shows that the average lifetimes detected at the fluorescence peak of 325 nm are longer than those detected at the fluorescence peak of 405 nm, when excited at 273 and 300 nm. This strongly indicates that the dual emissions centered at 325 and 405 nm do not originated from the combination of the intrinsic recombination radiation of carbogenic core and the relaxation of carriers onto the surface state. Furthermore, the average lifetimes of the C-dots studied here do not conform to the previously established mechanism, in which the average lifetime progressively lengthens with increasing emission wavelengths [30]. In addition, the dual emission at excitation below 300 nm suggests that the surface states are isolated without effective relaxation. Thus, we suggest that the pronounced slow decay of the PL dynamics at short-wavelength excitations (>14 ns) is likely due to the relaxation of the photogenerated carriers from carbogenic core onto the surface state. The fast decay at long-wavelength excitations (~1.3 ns) is attributed to a recombination of an electron–hole pair on surface site, in which the photogenerated carrier is directly excited from the surface state (Schematics of the carrier dynamics in C-dots, Fig. 4a). The slow recombination from carbogenic core onto the surface states is similar with surface-related emission in semiconductor quantum dots [31], and then might be attributed to the poor overlap of photogenerated electron from carbogenic core and hole wave function.

In the proposed schematic, different kinds of functional groups (C–O, C=O, C–H, C–OH) on the surface of the C-dots form different

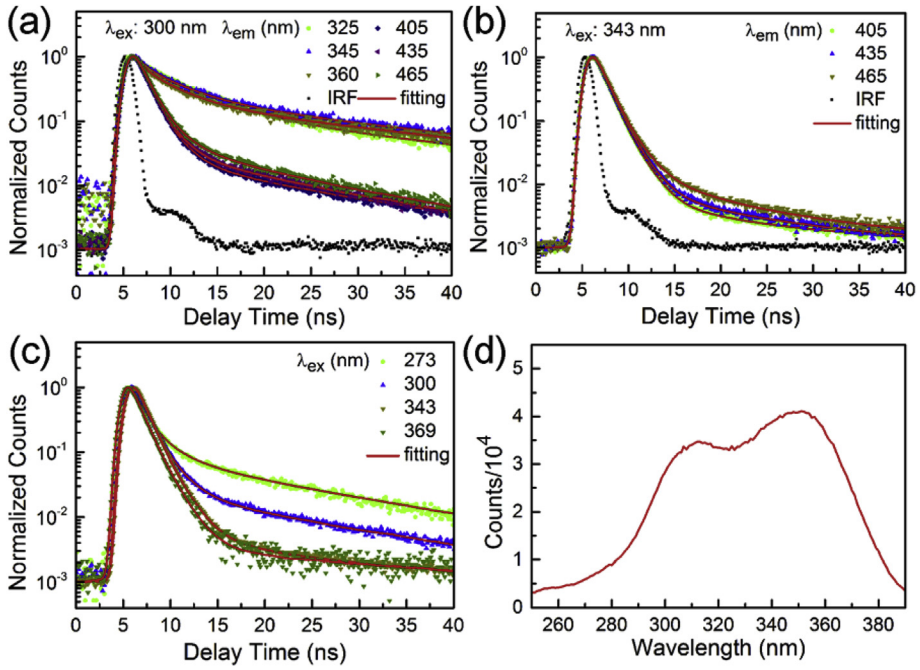

Fig. 3. Time-resolved PL spectra of as-prepared C-dots (a) at detection wavelengths of 325, 345, 360, 405, 435, and 465 nm with 300 nm excitation; (b) at detection wavelengths of 405, 435, and 465 nm with 343 nm excitation; (c) detected at 405 nm with excitation wavelengths of 273, 300, 343, and 369 nm (IRF: instrument response function). (d) Excitation spectrum of the C-dots detected at 405 nm. (A color version of this figure can be viewed online.)

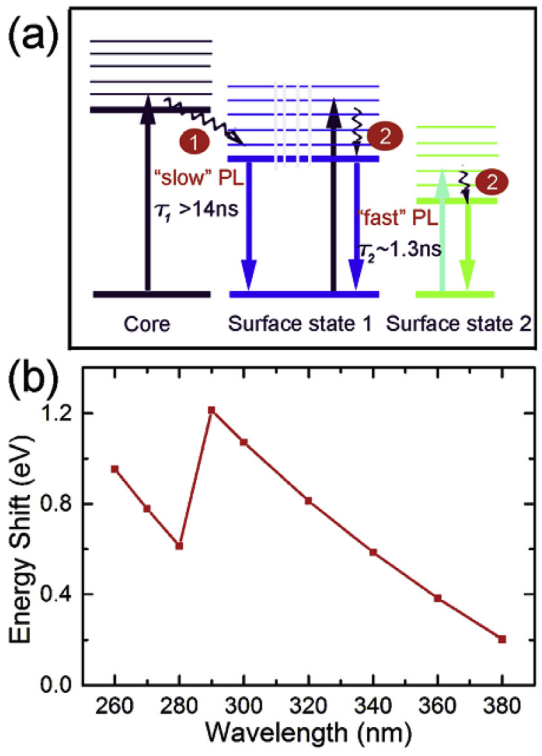

Fig. 4. (a) Schematics of the carrier dynamics in C-dots. There are two different pathways of electron–hole radiative recombination with distinct relaxation time scales: (1) relaxation of carriers from carbogenic core onto the surface states with a slow decay (τ_1 > 14 ns), (2) direct radiative recombination of the carriers on surface states with a fast decay (τ_2 ~ 1.3 ns). (b) The dependence of the energy shift (difference of excitation energy and emission energy) versus excitation wavelength. (A color version of this figure can be viewed online.)

surface state energy levels between energy level of carbogenic core [32]. The carbogenic core and a fraction of surface state (higher energy state) are excited simultaneously with a short-wavelength excitation. The relaxation from the carbogenic core onto the surface site and the direct radiative recombination inside surface states correspond to the slow and fast decays, respectively. The relaxation from the carbogenic core onto the surface site occurs when their energy levels are similar. There is a dominant slow decay at short-wavelength emissions and the average lifetime lengthens with increasing emission wavelengths. In contrast, the relaxation from the carbogenic core onto the surface site is ineffective at long-wavelength emissions and a fast decay is dominant.

Furthermore, the photogenerated carriers originating from carbogenic core decrease with increasing excitation wavelengths. Only the surface state (lower energy state) is excited when using a long-wavelength excitation where the energy is smaller than the band gap of the carbogenic core. Thus, the fast decay of the direct electron–hole radiative recombination localized on surface is dominant. As shown by the scheme in Fig. 4a, “Surface State 2” might be excited directly when using a long-wavelength excitation and the radiative recombination on this state is as fast as that on “Surface State 1”, i.e. 1.3 ns. In addition, a direct parallel between the length of the emission wavelength, i.e. deeper energy state, and the length of the average lifetime is expected when using an excitation of the same wavelength (as shown in Table 1).

For the C-dots studied here, two dominant emission centers, corresponding to the two fluorescence peaks, are excited when increasing the excitation wavelength. This leads to alternation of the dominant emission centers. This behavior is confirmed by observing the optimal emission energy, apparent in the dependence of the energy shift of the excitation on the excitation wavelength, shown in Fig. 4b. Two monotone decreasing curves are attributed to the excitation-independent fluorescence peaks of 325 and 405 nm, respectively. A sharp increase of the energy shift is observed when increasing the excitation wavelength from 280 to

290 nm. This indicates the transition of the dominant center from 325 to 405 nm, i.e. a change to a deeper emission center. Since all functional groups may become different emission centers [33], C-dots exhibit excitation-independent PL properties when the emission centers are uniform, i.e. has only one dominant emission center. However, only a small fraction of the deeper surface states can be excited using long-wavelength excitations because the excitation energy is smaller than the band gap of the dominant emission center. Subsequently, the fluorescence intensity decreases significantly. When the wavelengths are larger than 400 nm, the fluorescence peak of the C-dot emissions exhibits a red shift and excitation-dependence.

4. Conclusions

In conclusion, our analysis of the time-resolved PL from the C-dots suggests the existence of two different pathways of the electron–hole radiative recombination, each with a distinct relaxation time scale. At short wavelengths, a slow decay is dominant for the effective relaxation of carriers from carbogenic core onto the surface states. At long wavelengths, a fast decay is dominant for the direct radiative recombination of carriers on the surface states. Therefore, our two-pathway model proposed in this study provides a more thorough explanation than previous studies for the excitation-dependent and independent PL properties of C-dots.

Acknowledgments

This work was supported the by the National Basic Research Program of China (973 Program) under Grant No. 2012CB921804, and National Natural Science Foundation of China (Grant No. 61235003, 11304242 and 11474078), and Collaborative Innovation Center of Suzhou Nano Science and Technology. The TEM work was performed at the International Center for Dielectric Research (ICDR), Xi'an Jiaotong University, Xi'an, China. The authors also thank Mr. Ma and Ms. Lu for their help in using TEM.

References

[1] S.N. Baker, G.A. Baker, Luminescent carbon nanodots: emergent nanolights, Angew. Chem. Int. Ed. 49 (38) (2010) 6726–6744.
[2] H. Li, Z. Kang, Y. Liu, S. Lee, Carbon nanodots: synthesis, properties and applications, J. Mater. Chem. 22 (46) (2012) 24230–24253.
[3] X. Xu, R. Ray, Y. Gu, H.J. Ploehn, L. Gearheart, K. Raker, et al., Electrophoretic analysis and purification of fluorescent single-walled carbon nanotube fragments, J. Am. Chem. Soc. 126 (40) (2004) 12736–12737.
[4] S. Hu, K. Niu, J. Sun, J. Yang, N. Zhao, X. Du, One-step synthesis of fluorescent carbon nanoparticles by laser irradiation, J. Mater. Chem. 19 (4) (2009) 484–488.
[5] X. Li, H. Wang, Y. Shimizu, A. Pyatenko, K. Kawaguchi, N. Koshizaki, Preparation of carbon quantum dots with tunable photoluminescence by rapid laser passivation in ordinary organic solvents, Chem. Commun. 47 (3) (2011) 932–934.
[6] P. Hsu, H. Chang, Synthesis of high-quality carbon nanodots from hydrophilic compounds: role of functional groups, Chem. Commun. 48 (33) (2012) 3984–3986.
[7] H. Li, X. He, Y. Liu, H. Huang, S. Lian, S. Lee, et al., One-step ultrasonic synthesis of water-soluble carbon nanoparticles with excellent photoluminescent properties, Carbon 49 (2011) 605–609.
[8] S. Zhu, Q. Meng, L. Wang, J. Zhang, Y. Song, H. Jin, et al., Highly photoluminescent carbon dots for multicolor patterning, sensors, and bioimaging, Angew. Chem. Int. Ed. 52 (14) (2013) 3953–3957.
[9] R. Fan, Q. Sun, L. Zhang, Y. Zhang, A. Lu, Photoluminescent carbon dots directly derived from polyethylene glycol and their application for cellular imaging, Carbon 71 (2014) 87–93.
[10] J. Tang, B. Kong, H. Wu, M. Xu, Y. Wang, Y. Wang, et al., Carbon nanodots featuring efficient FRET for real-time monitoring of drug delivery and two-photon imaging, Adv. Mater. 25 (45) (2013) 6569–6574.
[11] Z. Ma, Y. Zhang, L. Wang, H. Ming, H. Li, X. Zhang, et al., Bioinspired photoelectric conversion system based on carbon-quantum-dot-doped dye-semiconductor complex, ACS Appl. Mater. Interfaces 5 (11) (2013) 5080–5084.
[12] X. Zhang, Y. Zhang, Y. Wang, S. Kalytchuk, S.V. Kershaw, Y. Wang, et al., Color-switchable electroluminescence of carbon dot light-emitting diodes, ACS Nano 7 (12) (2013) 11234–11241.
[13] X. Guo, C.F. Wang, Z.Y. Yu, L. Chen, S. Chen, Facile access to versatile fluorescent carbon dots toward light-emitting diodes, Chem. Commun. 48 (21) (2012) 2692–2694.
[14] F. Wang, Y. Chen, C. Liu, D. Ma, White light-emitting devices based on carbon dots' electroluminescence, Chem. Commun. 47 (12) (2011) 3502–3504.
[15] W.F. Zhang, H. Zhu, S.F. Yu, H.Y. Yang, Observation of lasing emission from carbon nanodots in organic solvents, Adv. Mater. 24 (17) (2012) 2263–2267.
[16] M.J. Krysmann, A. Kelarakis, P. Dallas, E.P. Giannelis, Formation mechanism of carbogenic nanoparticles with dual photoluminescence emission, J. Am. Chem. Soc. 134 (2) (2012) 747–750.
[17] P. Yu, X. Wen, Y. Toh, J. Tang, Temperature-dependent fluorescence in carbon dots, J. Phys. Chem. C 116 (48) (2012) 25552–25557.
[18] X. Wen, P. Yu, Y. Toh, X. Hao, J. Tang, Intrinsic and extrinsic fluorescence in carbon nanodots: ultrafast time-resolved fluorescence and carrier dynamics, Adv. Opt. Mater. 1 (2) (2013) 173–178.
[19] V. Strauss, J.T. Margraf, C. Dolle, B. Butz, T.J. Nacken, J. Walter, et al., Carbon nanodots: toward a comprehensive understanding of their photoluminescence, J. Am. Chem. Soc. 136 (49) (2014) 17308–17316.
[20] K. Hola, A.B. Bourlinos, O. Kozak, K. Berka, K.M. Siskova, M. Havrdova, et al., Photoluminescence effects of graphitic core size and surface functional groups in carbon dots: COO- induced red-shift emission, Carbon 70 (2014) 279–286.
[21] L. Bao, Z. Zhang, Z. Tian, L. Zhang, C. Liu, Y. Lin, et al., Electrochemical tuning of luminescent carbon nanodots: from preparation to luminescence mechanism, Adv. Mater. 23 (48) (2011) 5801–5806.
[22] Y. Long, C. Zhou, Z. Zhang, Z. Tian, L. Bao, Y. Lin, et al., Shifting and non-shifting fluorescence emitted by carbon nanodots, J. Mater. Chem. 22 (13) (2012) 5917–5920.
[23] V. Nguyen, L. Yan, J. Si, X. Hou, Femtosecond laser-induced size reduction of carbon nanodots in solution: effect of laser fluence, spot size, and irradiation time, J. Appl. Phys. 117 (8) (2015) 84304.
[24] D. Tan, S. Zhou, J. Qiu, N. Khusro, Preparation of functional nanomaterials with femtosecond laser ablation in solution, J. Photochem. Photobiol. C 17 (2013) 50–68.
[25] D. Werner, A. Furube, T. Okamoto, S. Hashimoto, Femtosecond laser-induced size reduction of aqueous gold nanoparticles: in situ and pump-probe spectroscopy investigations revealing coulomb explosion, J. Phys. Chem. C 115 (17) (2011) 8503–8512.
[26] Z. Xu, L. Yang, X. Fan, J. Jin, J. Mei, W. Peng, et al., Low temperature synthesis of highly stable phosphate functionalized two color carbon nanodots and their application in cell imaging, Carbon 66 (2014) 351–360.
[27] Y. Feng, J. Zhao, X. Yan, F. Tang, Q. Xue, Enhancement in the fluorescence of graphene quantum dots by hydrazine hydrate reduction, Carbon 66 (2014) 334–339.
[28] S. Hu, R. Tian, Y. Dong, J. Yang, J. Liu, Q. Chang, Modulation and effects of surface groups on photoluminescence and photocatalytic activity of carbon dots, Nanoscale 5 (23) (2013) 11665–11671.
[29] D. Tan, S. Zhou, B. Xu, P. Chen, Y. Shimotsuma, K. Miura, et al., Simple synthesis of ultra-small nanodiamonds with tunable size and photoluminescence, Carbon 62 (2013) 374–381.
[30] X. Wen, P. Yu, Y.R. Toh, X. Ma, J. Tang, On the upconversion fluorescence in carbon nanodots and graphene quantum dots, Chem. Commun. 50 (36) (2014) 4703–4706.
[31] X.Y. Wang, L.H. Qu, J.Y. Zhang, X.G. Peng, M. Xiao, Surface-related emission in highly luminescent CdSe quantum dots, Nano Lett. 3 (8) (2003) 1103–1106.
[32] L. Tang, R. Ji, X. Cao, J. Lin, H. Jiang, X. Li, et al., Deep ultraviolet photoluminescence of water-soluble self-passivated graphene quantum dots, ACS Nano 6 (6) (2012) 5102–5110.
[33] L. Wang, S. Zhu, H. Wang, S. Qu, Y. Zhang, J. Zhang, et al., Common origin of green luminescence in carbon nanodots and graphene quantum dots, ACS Nano 8 (3) (2014) 2541–2547.